# Time-Domain Asymptotic Solutions in the Transition Regions near Geometrical Boundaries and near Caustics for Scattering by a Dielectric Cylinder

Teruhiko Ida* and Toyohiko Ishihara

Department of Communication Engineering, National Defense Academy, Hashirimizu, Yokosuka, 239-8686 Japan

## I. Introduction

The studies on the scattering of electromagnetic fields by a dielectric cylinder have been an important research subject for a variety of applications in the area of antennas and propagation [1]-[6]. The scattered fields by a dielectric cylinder have been calculated numerically by applying the eigenfunction representation, the method of moment, and so on. However, such methods may not be effective for the problems when the radius of curvature is sufficiently larger than the wavelength.

In this study, a time-domain asymptotic analysis is discussed for the scattered electromagnetic fields when the cylindrical wave radiated from a magnetic line source is incident on a dielectric cylinder. We assume the Gaussian-type modulated pulse source whose spectrum is distributed in the high-frequency domain. The time-domain scattered field solutions derived in this paper are applicable in the transition regions near the geometrical boundaries, produced by the incident ray on the dielectric cylinder from the tangential direction, and near the caustics, produced by the family of the reflected ray group on the concave side of the dielectric cylinder. Comparisons of the time-domain asymptotic solution with the reference solution calculated numerically from a combination of the eigenfunction representation and the First Fourier Transform(FFT) code confirm the validity and the utility of the proposed time-domain asymptotic solution.

## II. Frequency-Domain Asymptotic Solutions

### 1. Formulation and scattering phenomena

Fig.1 shows the dielectric cylinder with the radius of curvature $a$ and the dielectric constant $\varepsilon_2$, and the cylindrical coordinate system $(\rho, \phi, z)$ and the cartesian coordinate system $(x, y, z)$. When the dielectric cylinder is illuminated by an incident wave radiated from a magnetic line source $Q(\rho_0, \phi_0)$, the frequency-domain scattered magnetic field observed at the point $P(\rho, \phi)$ can be obtained from the eigenfunction expansion [1] [2].

When the Watson transform [1],[5],[6] is applied to the eigenfunction representation, one may obtain the integral representation for the scattered field. Various high-frequency

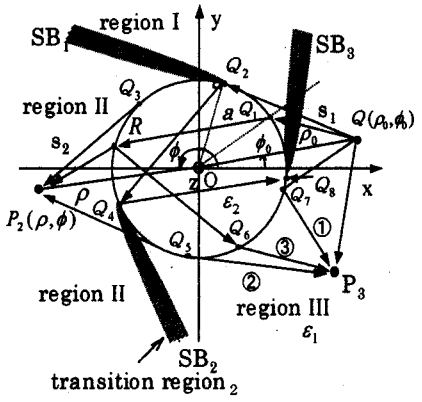


Fig.1 Schematic figure for scattering by a dielectric cylinder with the radius of curvature $a$ and the coordinate system $(\rho, \phi, z)$. $Q(\rho_0, \phi_0)$ : magnetic line source, $P(\rho, \phi)$ : observation point.

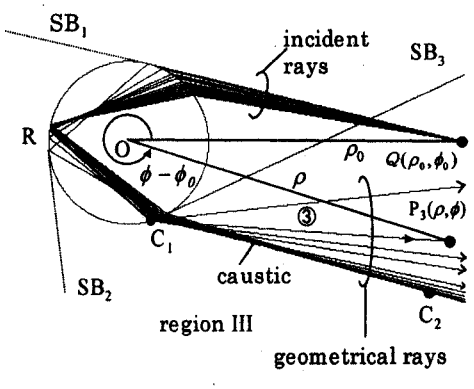


Fig.2 The caustic $C_1C_2$ constructed by the family of the once reflected ray group on the concave boundary of the dielectric cylinder

solutions can be derived from this integral representation. In Fig.1, the scattering phenomena are shown schematically. The observation region in the surrounding air is divided into the three regions I–III, in this example, by the geometrical shadow boundaries

0-7803-7846-6/03/$17.00 ©2003 IEEE

$SB_1$–$SB_3$. The shadow boundary $SB_1$ is produced by the direct ray $\overline{QQ_2}$ incident on the dielectric cylinder from the tangential direction. The $SB_2$ is produced by the refracted ray $\overline{Q_2Q_4}$, excited by the tangential ray $\overline{QQ_2}$, at the point $Q_4$. Similarly, the $SB_3$ is produced by the refracted ray $\overline{Q_4Q_8}$, refracted at $Q_2$ and reflected on the concave boundary at $Q_4$. The similar scattering phenomena are observed within the same region divided by the shadow boundaries. For example, the direct ray $\overline{QP_3}$, the reflected ray ①, the refracted-refracted-surface diffracted ray ② ( $Q \to Q_2 \to Q_4 \to Q_5 \to P_3$ ) and the transmitted-reflected-transmitted ray ③ ($Q \to Q_1 \to R \to Q_6 \to P_3$ ) are observed at the point $P_3$ located in the region III.

## 2. Modified uniform GTD(UTD) solution near the $SB_1$

The surface diffracted ray $\overline{QQ_2} \to \overset{\frown}{Q_2Q_3} \to \overline{Q_3P_2}$ observed in the transition region ( shaded region ) near the shadow boundary $SB_1$ and in the region II ( see Fig.1 ) can be calculated from the following modified UTD solution:

$$H_{z,s} \sim G(k_1 s_1)\{\sum_{m=1}^{\infty} D_m(Q_2)A_m(Q_2)\exp(ik_1\bar{l} - \Omega_m\bar{l})D_m(Q_3)A_m(Q_3)\}G(k_1 s_2) \tag{1}$$

$$G(k_1 s_{1,2}) = \exp(ik_1 s_{1,2} + i\pi/4)/(8\pi k_1 s_{1,2})^{1/2} \ , \ \bar{l} = a\theta \ , \ \theta = \angle Q_2OQ_3 \tag{2}$$

$$D_m(Q_{2,3}) = \sqrt{\frac{2M}{\sigma_m}}\exp(-i\frac{\pi}{12})\frac{1}{Ai(-\sigma_m)}\frac{1}{\sqrt{\alpha_m}} \ , \ \Omega_m = M\sigma_m a^{-1}\exp(-i\pi/6) \tag{3}$$

$$A_m(Q_{2,3}) = \exp[\{M^2\sigma_m^2\exp(i7\pi/6)\}/\{2k_1 s_{1,2}\}] \ , \ M = (k_1 a/2)^{1/3} \tag{4}$$

$$\alpha_m = 1 + \sqrt{\frac{\varepsilon_1}{\varepsilon_2}}\exp(-i\frac{\pi}{2})/(k_2 a)\{\frac{\sqrt{(k_2a)^2 - \nu_m^2}W_1'(\tau_m)M}{\tau_m W_1(\tau_m)} - \frac{\nu_m M^2}{\tau_m\sqrt{(k_2a)^2 - \nu_m^2}}\} \tag{5}$$

where $A_m(Q_{2,3})$ denotes the coefficient to modify the conventional GTD's diffraction coefficient $D_m(Q_{2,3})$ and $W_1(= Ai - iBi)$ the Airy function. The eigenvalues $\sigma_m$, and corresponding $\tau_m$ and $\nu_m$ are calculated from the following equations.

$$Ai'(-\sigma_m) - \exp(-i\frac{\pi}{6})MAi(-\sigma_m)\sqrt{\frac{\varepsilon_1}{\varepsilon_2}}\sqrt{1 - \{\frac{k_1 a + M\sigma_m\exp(i\pi/3)}{k_2 a}\}^2} = 0 \tag{6}$$

$$\tau_m = \sigma_m\exp(i\pi/3) \ , \ \nu_m = k_1 a + M\tau_m. \tag{7}$$

## 3. Transmitted fields solution near the $SB_2$

When the observation point $P_2$ is located in the transition region 2 (see Fig.1), the geometrical ray solution for the transmitted ray ($Q \to Q_1 \to R \to P_2$) can not be applied since the Debye's approximations for the cylindrical functions used to derive the conventional transmitted ray are not applicable for this case. The transmitted field solution may be calculated from the following representation:

$$H_{z,t} = G(k_1 s_1)\exp(2ik_2 a\cos\theta_t + ik_1\bar{\ell})G(k_1 s_2)\hat{C}oI(\hat{\xi}), \hat{C}o = 8M^2(\varepsilon_1/\varepsilon_2)^{1/2}\cos\theta_t/\pi \tag{8}$$

$$I(\hat{\xi}) = \int_{-\infty}^{\infty}\frac{\exp\{i\hat{\xi}\tau + i(\frac{M^2}{2k_1 s_1} + \frac{M^2}{2k_1 s_2} + \frac{2M^2}{2k_2 a\cos\theta_t})\tau^2\}}{\{W_1'(\tau) + \sqrt{(\varepsilon_1/\varepsilon_2)}Mh(\tau)W_1(\tau)\}^2}d\tau \ , \ \hat{\xi} = M(\hat{\theta} - 2\hat{\phi}) \tag{9}$$

$$h(\tau) = H_\nu^{(2)\prime}(k_2 a)/H_\nu^{(2)}(k_2 a) \sim \sqrt{(k_2a)^2 - (k_1 a + M\tau)^2}\exp(-i\pi/2)/(k_2 a) \tag{10}$$

where $\hat{\theta} = \angle Q_2OQ_5$ and $2\hat{\phi} = \angle Q_2OQ_4$, measured in the counterclockwise direction, and $\theta_t = \angle OQ_2Q_4$ is the critical refraction angle. The integral in (9) can be calculated very quickly by deforming the integration contour and by performing the numerical integration applying the Simpson formula.

## 4. Ray solution near the caustic $C_1C_2$

When the observation point is located at $P_3$ in the region III, the geometrical ray ③ is observed ( see Fig.1 ). However, a family of these ray group constructs the caustic $C_1C_2$ as shown in Fig.2. Thus, the conventional geometrical ray solution can not be applied in the transition region near this caustic. The asymptotic solution obtained from the integral representation by taking into account the two adjacent first-order saddle points is represented as follows.

$$H_{s,c} \sim \frac{i\pi}{8}\frac{\exp[ik_1\{q(w_1)+q(w_2)\}/2]}{k_1^{1/3}}\eta^{1/4}[F_1 Ai(-\eta k_1^{2/3}) + iF_2\frac{Ai'(-\eta k_1^{2/3})}{\eta^{1/2}k_1^{1/3}}] \tag{11}$$

$$q(w_j) = \sqrt{\rho_0^2 - (a\sin w_j)^2} + \sqrt{\rho^2 - (a\sin w_j)^2} + 4a\sqrt{(\varepsilon_1/\varepsilon_2)^2 - (\sin w_j)^2} - 2a\cos w_j \ , \ j=1,2 \ , \ \eta = [(3/4)\{q(w_1)-q(w_2)\}]^{2/3} \tag{12}$$

$$F_{1,2} = f(w_1)\sqrt{-2/\{iq''(w_1)\}} \pm f(w_2)\sqrt{2/\{iq''(w_2)\}} \tag{13}$$

$$q''(w_j) = \frac{4a^2\cos^2 w_j}{\sqrt{(k_1/k_2)^2 - \sin^2 w_j}} + \frac{a\cos^2 w_j}{\sqrt{(\rho_0/a)^2 - \sin^2 w_j}} + \frac{a\cos^2 w_j}{\sqrt{(\rho/a)^2 - \sin^2 w_j}} - 2a\cos w_j \tag{14}$$

$$f(w_j) = T_{12}(w_j)T_{21}(w_j)R_{22}(w_j)\frac{2k_1 a\cos w_j \exp(-i\pi/2)}{\pi k_1\{\rho_0^2 - (a\sin w_j)\}^{1/4}\{\rho^2 - (a\sin w_j)\}^{1/4}} \tag{15}$$

where $T_{12(21)}(w_j)$ denotes the transmission coefficient from the air to the dielectric cylinder(from the dielectric cylinder to the air) and $R_{22}(w_j)$ the reflection coefficient at the point $R$ (see Figs.1 and 2) on the concave boundary [1],[6]. These coefficients agree with the Fresnel transmission coefficients and the reflection coefficient, respectively, if the saddle points $w_j, j=1,2$, are not located near $\pi/2$. The two saddle points $w_j, j=1,2$, are obtained from the saddle point equation:

$$|\phi - \phi_0| = 4(\pi/2 - \sin^{-1}(k_1/k_2)\sin w_j) + (\pi/2 - \sin^{-1}(a/\rho_0)\sin w_j) + (\pi/2 - \sin^{-1}(a/\rho)\sin w_j) - 2(\pi/2 - w_j) \tag{16}$$

## III. Time-Domain Asymptotic Solutions

We will apply the Gaussian-type modulated pulse source $s(t)$ (see Fig.3) defined as

$$s(t) = \{U(t) - U(t-2t_0)\}\exp\{-i\omega_0(t-t_0) - (t-t_0)^2/(4d^2)\} \tag{17}$$

where $U(t)$ denotes the unit step function.

When a dielectric cylinder is illuminated by the incident wave excited by the pulse source in (17), the time-domain asymptotic solution $y(t,\rho,\phi)(\equiv y(t))$ for the scattered field can be obtained from the inverse Fourier transform of the product of the frequency-domain scattered field solution $H_z^s(\omega)$ and the frequency spectrum $S(\omega)$ of the source function $s(t)$ in (17) as follows,

$$y(t) = \frac{1}{2\pi}\int_{-\infty}^{\infty} H_z^s(\omega)S(\omega)\exp(-i\omega t)d\omega. \tag{18}$$

The frequency-domain scattered field solution $H_z^s(\omega)$ consists of the several terms $H_{s,i}(\omega)(i=1,2,\cdots)$ such as the reflected ray ① $(i=1)$, the surface diffracted ray ② $(i=2)$, the reflected ray ③ $(i=3)$, and so on (see Fig.1). Each term $H_{s,i}(\omega)$ constructing the total response waveform can be expressed as $H_{s,i}(\omega) = A_i(\omega)\exp(i\omega L_i/c_1)$, where $c_1$ denotes the speed of light in the air, $L_i$ the distance parameter, and $A_i(\omega)$ the slowly varying amplitude as the function of $\omega$. When $S(\omega)$ and $H_{s,i}(\omega)$ are substituted into the inverse Fourier transform in (18), one may obtain

$$y_i(t) = (d/\sqrt{\pi})\exp\{-i\omega_0 T_i - T_i^2/(2d)^2\}\hat{I}_i(d) \ , \ T_i = t - t_0 - L_i/c \tag{19}$$

$$\hat{I}_i(d) = \int_{-\infty}^{\infty} F_i(\omega)\exp\{-d^2\hat{q}_i(\omega)\}d\omega \ , \ F_i(\omega) = A_i(\omega)\mathrm{Re}[\mathrm{erf}\{\beta(\omega)\}] \tag{20}$$

$$\hat{q}_i(\omega) = \{\omega - \omega_0 + iT_i/(2d^2)\}^2 \ , \ \beta(\omega) = (t_0/2d)^2 - id(\omega - \omega_0) \tag{21}$$

The integral in (20) can be evaluated asymptotically assuming $d^2 >> 1$. Then, the time-domain asymptotic solution is obtained from the following representation:

$$y_i(t) = s(t - L_i/c_1)A_i(\omega_{s,i})\mathrm{Re}[\beta(\omega_{s,i})] \ , \ \omega_{s,i} = \omega_0 - iT_i/(2d^2) \tag{22}$$

## IV. Numerical Results and Discussions

In Fig.4, we have compared the frequency-domain asymptotic solution in Sec. II with the exact solution calculated from the eigenfunction representation. The scattered field magnitude curve is drawn as the function of the angular distance $|\phi - \phi_0|$. The asymptotic solution (solid curve) agrees excellently with the exact solution (dotted curve).

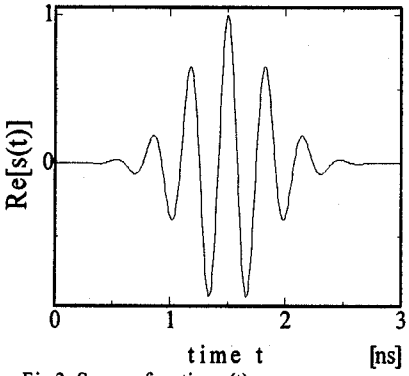


Fig.3 Source function s(t).
$\omega_0 = 3.0 \times 10^9$, $t_0 = 15 \times 10^{-10}$, $d = 25 \times 10^{-11}$

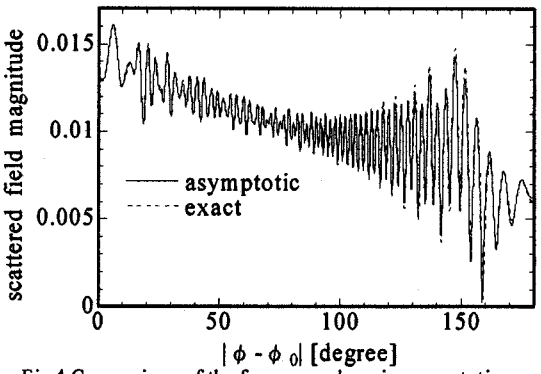


Fig.4 Comparison of the frequency-domain asymptotic solution with the exact solution. Numerical parameters : $a = 0.6$, $\varepsilon_2 = 3.0$, $\rho_0 = 2.52$, $\rho = 6.0$, $f = 3$GHz

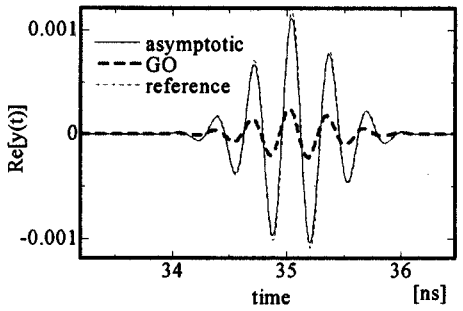


Fig.5 Transmitted pulse wave observed at $P_2(6.0, 265^\circ)$ near the $SB_2$ ($\rho = 6.0$, $|\phi - \phi_0| = 269.96^\circ$) in the region II.

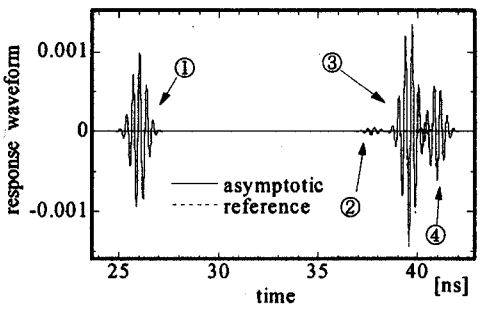


Fig.6 Time-domain scattered fields observed at $P_3(6.0, 339.8^\circ)$ near the caustic $C_1C_2$ ($\rho = 6.0$, $|\phi - \phi_0| = 340^\circ$) in the region III.

Fig.5 shows the transmitted pulse wave observed near the shadow boundary $SB_2$ in the region II (see Fig.1) when the pulse wave in (17) is incident on the dielectric cylinder. The asymptotic solution calculated by using (22) and (8) agrees very well with the reference solution calculated numerically from (18) by using the FFT. The conventional geometrical ray solution shown by the bold dotted curve shows the large error near the $SB_2$.

The total time-domain scattered field observed near the caustic $C_1C_2$ in the region III (see Figs.1 and 2) is shown in Fig. 6. The response waveforms ① ~ ③ shown in Fig.6 correspond, respectively, to the reflected ray ①, the surface diffracted ray ②, and the reflected ray ③ in Fig.1. The response waveform ④ in Fig.6 is not shown in Fig.1 in order to avoid the crowded figure. The asymptotic solution agrees excellently with the reference solution calculated numerically.

## V. Conclusion

We have derived the time-domain asymptotic solutions for the scattered fields by the dielectric cylinder. The new solutions can be applied near various kinds of the geometrical boundaries and the ray caustics. By comparing the asymptotic solutions with the reference solution calculated numerically, we have confirmed the validity of the proposed asymptotic solution and clarified the scattering phenomena by a dielectric cylinder.

## References

[1] Y. M. Chen, J. Math. Phys., Vol.5, No.6, pp.820-832,1964.
[2] H. M. Nussenzbeig, J. Math. Phys., Vol.10, No.1, pp.82-124, 1969.
[3] E. Heyman and L. B. Felsen, IEEE, Trans. on Antennas and Propag., Vol. AP-32, No.9, pp.969-978,1984.
[4] H. Ikuno, T. Ohmori, and M. Nishimoto, Trans. on IEICE, J76-C-1, pp.119-129,1993.
[5] T. Sasamori, T. Uno, and S. Adachi, Trans. on IEICE, J78-C-I, pp.9-19,1995.
[6] T. Ida and T. Ishihara, the paper of Technical Meeting on EMT, IEE, Japan, EMT-02-72, pp.65-70, 2002.